A Study of Geometry and Commercial Off-The-Shelf (COTS) Antennas for Controlled Reception Pattern Antenna (CRPA) Arrays

Yu-Hsuan Chen, *Stanford University, U.S.A.*

BIOGRAPHY

Yu-Hsuan Chen is a visiting student in the GPS Laboratory at Stanford University since 2010. He received his M.S. degree in electrical engineering from National Cheng Kung University, Taiwan in 2002. His research interests include real-time GNSS software receiver design and its application of antenna-array beam-forming, dual frequency and scintillation.

ABSTRACT

Controlled Reception Pattern Antenna array (CRPA) is an effective approach for rejecting interference and enhancing the received GNSS signal power. Conventionally, the antenna array used for CRPA is designed for reducing imbalance between elements. Additionally, full calibration should be made for calculating the spacing between elements and the cabling latency before performing CRPA. Hence, the high cost and complex calibration of antenna arrays decrease the attractiveness of CRPA to many user communities. We develop an approach which can perform CRPA without any prior information. Specifically, inexpensive and Commercial Off-The-Shelf (COTS) antennas can be used as elements of an antenna array. This allows the elements to be easily arranged to any desired array layout. With this new freedom in array geometry, the important issue of its effect on performance is raised. As the characteristics of antenna and array layout will affect the anti-interference performance, it is important to study the effect of antenna array geometry and select the best units/layouts combination.

In this study, we examined both COTS antenna use and the effect of array geometry by assessing three models of commercial antennas and arranging these in two selected layouts. The antenna patterns of two physical layouts are analyzed in terms of beamwidth and illustrated. Signal collection hardware is built to record the data sets of antenna array. A positioning procedure of calculating electrical layout is developed using differential carrier phase measurements. We collected data sets for each antenna/layout combination. And, these data sets are processed by our software receiver to log the carrier phase measurements. The electrical layouts determined from the positioning procedure are compared with physical ones for examining the mutual coupling effects on the antenna array. From these results, we can assess the array layouts and the COTS antennas

INTRODUCTION

Global Navigation Satellite System (GNSS) signals are relatively weak and thus vulnerable to deliberate or unintentional interference. An electronically-steered antenna array system provides an effective approach to mitigate interference by controlling the reception pattern and steering beams/nulls. As a result, so-called Controlled Reception Pattern Antenna (CRPA) array have been deployed by organizations such as the US Department of Defense which seeks high levels of interference rejection.

Our efforts have focused on developing a commercially viable CRPA system using Commercial Off-The-Shelf (COTS) components to support the needs of Federal Aviation Administration (FAA) alternative position navigation and timing (APNT) efforts. In 2010, we implemented a 7-element, 2-bit-resolution, single-beam and real-time CRPA software receiver [1]. In 2011, the receiver was upgraded to support all-in-view, 16-bit-resolution and 4-element. Even though we can implement all these CRPA software receivers in real time, the performance of anti-interference is highly dependent on the antenna array layout and characteristic of antenna element. Our beamforming approach allows us to utilize several COTS antennas as array rather than custom designed and fully calibrated antenna [2]. The use of COTS antenna is important as the goal of the effort is to develop CRPA for commercial endeavors - specifically robust timing for the national airspace. Hence, it is important to study the geometry layout of the individual antennas of the array to assess the layouts and how antenna performance affect the results. We adopted three models of COTS antenna and two possible layouts for a 4-element array. Then, signal collection hardware

consisting of 4 Universal Software Radio Peripheral (USRP) [3] and one host Personal Computer (PC) is built to collect array data sets for each layout/antenna combination. Our developed CRPA software receiver is used to process all data sets and output carrier phase measurements. We address a procedure to calculate the electrical layouts of antenna array by differential carrier phase positioning. When compared to physical layout, the results of electrical layouts can be used to determine the mutual coupling effect of each combination. Using the electrical layout, the resultant gain patterns can be calculated and used to see the beamwidth and side lobe issue. This is important as these factors have significant effect on anti-interference performance. This study focuses on understanding the performance effects of geometry and developing a method for describing the best geometry.

This paper is organized as follows. First, pattern analysis for two selected layouts is provided. Then, the specifications of COTS antennas are listed. The signal collection hardware and experimental setups are described in detail. The approach for logging carrier phase measurement by our developed CRPA receiver is explained. For calculating the electrical layout, a procedure to solve the spacing between elements is provided. The calculated results of electrical spacing for all layouts are compared to physical layout. And, the resulting patterns are shown for discussing the mutual coupling effect of antenna. Finally, some concluding remarks are made.

PATTERN ANALYSIS OF ANTENNA ARRAY

Pattern is defined as the directional strength of radio frequency signal from the antenna. The pattern of antenna array is the product of the isotropic array factor and the isolated element pattern. We assume that the pattern of each element is identical and only consider the isotropic array factor. Figure 1 shows the coordination of an antenna array. First element is set as reference position. The x-axis is the east direction, y axis is the north direction and z axis is up direction. $\vec{p}_{i1}$ is the baseline vector of the *i*th antenna. $\hat{r}$ is the unit vector to satellite.

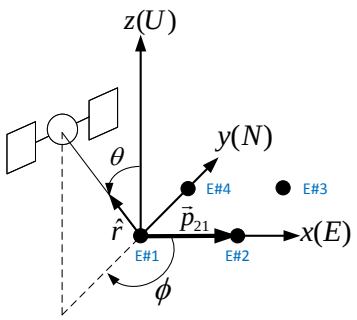

Figure 1. Antenna geometry and direction of satellite

The isotropic array factor is given by [4]

$$GP(\phi,\theta) = \sum_{i=1}^{M} A_i \exp\left[j\left(\frac{2\pi \vec{p}_{i1} \cdot \hat{r}_l(\phi,\theta)}{\lambda} \right) \right] \qquad (1)$$

where λ is wavelength, and A_i is a complex constant. Currently, we only implement a 4-element array CRPA software receiver in real time. Hence, we analyze two kinds of layout of half-wavelength 4-element array 1) symmetrical Y and 2) square. Each antenna is separated from its nearest neighbor by half wavelength. Figure 2 shows the photos of two layouts. Figure 3 shows its physical layouts.

Figure 2. Photos of antenna array
Left: Y and Right: square

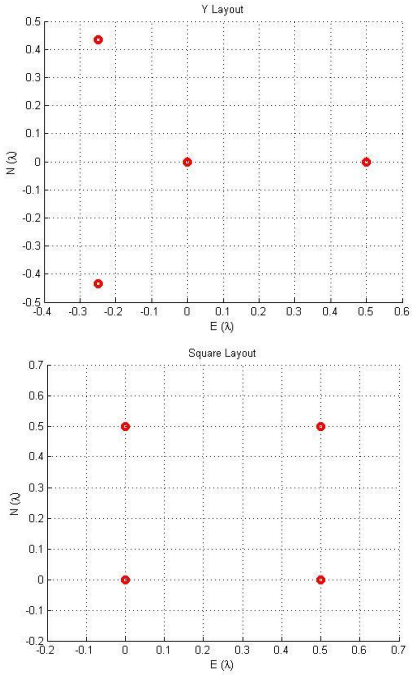

Figure 3. Physical layout of antenna array
Top: Y and Bottom: square

The antenna patterns towards the direction of elevation 90º are shown in the figure 3. One of key characteristic of pattern is the beamwidth which is defined as the angle with 3dB loss. Figure 4 shows the pattern along elevation where the beamwidth of Y layout is 74º and 86º for square layout. Narrow beamwidth will benefit anti-interference performance particularly if the interference is close to the direction of the target satellite.

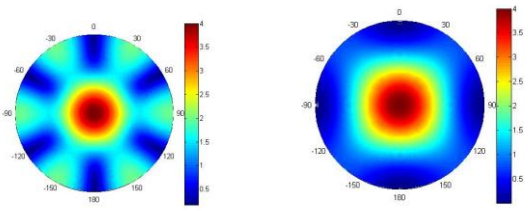

Figure 3. Patterns of antenna array Left: Y and Right: square

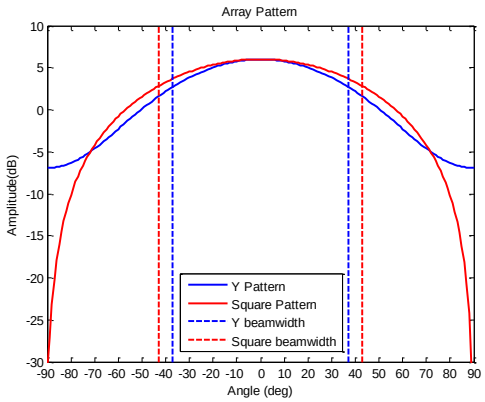

Figure 4. Beamwidth of patterns of Y and square layouts (3 dB beamwidth shown)

SPECIFICATIONS OF COTS ANTENNAS

Typically, the COTS antenna selection is determined by high gain and great out-of-band rejection. Table 1 shows specifications of three models of antenna which are used in this paper [5]. These antennas are the patch antennas. The SAW filters are equipped for rejecting out-of-band signal. The 3-stage Low Noise Amplifiers (LNA) with over 30 dB gain are also embedded.

Table 1. Specifications lists of COTS antennas

Spec \ Ant	Antenna #1 WS3978	Antenna #2 3978D-HR	Antenna #3 WS3997
RF Frequency	1572.5 ~ 1578 MHz	1575.42 ±10MHz	1572.5 ~ 1578 MHz
Antenna Gain	@90º 3dBic @20º-2dBic	@90º 3dBic @20º-2dBic	@90º 3dBic @20º-2dBic
LNA Gain	40 dB	40 dB	30 dB
LNA Noise Figure	3.1 dB	0.5 dB	1.5 dB
Out-of-band rejection	± 40 MHz: 35 dB	± 40 MHz: 35 dB	±15 MHz: 5 dB ± 20 MHz: 10 dB ± 30 MHz: 32 dB ± 40 MHz: 40 dB

DESCRIPTION OF SIGNAL COLLECTION HARDWARE AND EXPERIMENTAL SETUPS

The hardware used to collect the antenna array datasets is depicted in figure 5. Its photo is shown in figure 6. The hardware contains 4-element antenna array, four USRP2 software radio systems [3] and one host computer. The signal received from the COTS antenna passes to a USRP2 board equipped with a DBSRX2 programmable mixing and down-conversion daughterboard. The individual USRP2 boards are synchronized by a 10 MHz external common clock generator and Pulse Per Second (PPS) signal. The USRP2s are controlled by a host computer running the Ubuntu distribution of Linux. The open-source GNU Radio software-defined radio block is used to configure USRP2 and collect dataset. All USRP2s are configured to collect L1 (1575 MHz) signal. The signals are converted to near zero Intermediate Frequency (IF) and digitized to 14-bit complex outputs (I & Q). Its sampling rate is set as 4 MHz. The host computer uses two solid state drives for storing the data set. For this study, 64 Megabyte/s (MB/s) is needed. The fast solid state drives are especially useful when using high bandwidth signals such as L5 which will require very high data streaming rate (80 MB/sec/channel).

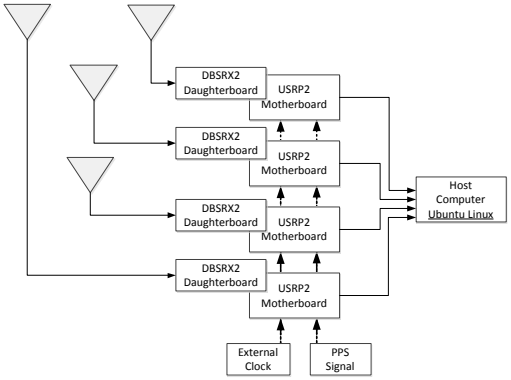

Figure 5. Block diagram of the signal collection hardware

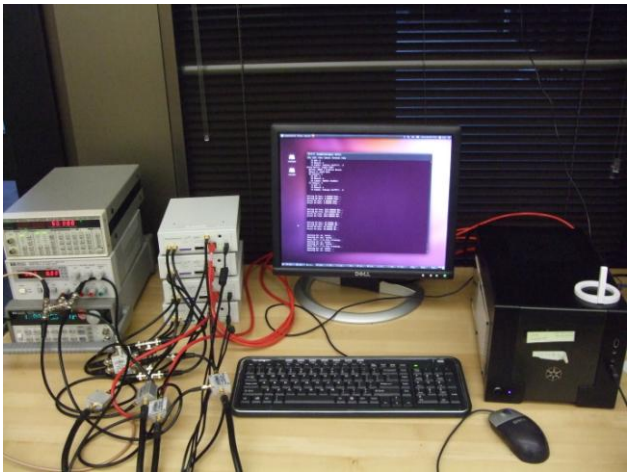

Figure 6. Photo of the signal collection hardware

In order to compare physical and electrical layout of antenna array, we set up the signal collection hardware to record six data sets for 2 layouts and 3 antenna models shown in table 2. All the data sets are 5 minutes long to obtain enough carrier phase measurements for positioning.

Table 2. Experimental setups

Data set #	Antenna array layout	Antenna model
1	Y	WS3978
2	Y	3978D-HR
3	Y	WS3997
4	Square	WS3978
5	Square	3978D-HR
6	Square	WS3997

LOGGING CARRIER PHASE MEASUREMENTS FROM CRPA SOFTWARE RECEIVER

In order to calculate the precise spacing between elements, the hundreds of seconds of carrier phase measurements for each element are needed. The collected data sets are processed by our developed CRPA software receiver. The software receiver is developed with Visual Studio under Windows. Most of source code is programmed using C++. Assembly language is used to program the functions with high computational complexity such as correlation operations. The software architecture of CRPA software receiver is depicted in the figure 7 [1][6][7][8]. This architecture exploits four sets of 12 tracking channels in parallel to process each IF signal from antenna element. Each channel is dedicated to track the signal of single satellite. The tracking channels output carrier phase measurements to build the steering vectors for each satellite. Minimum Variance Distortionless Response (MVDR) algorithm is adopted for calculating the weights adaptively. Here, there are 12 weights sets, one for each satellite in a tracking channel, for desired directions of satellites. Using the pre-correlation beamforming approach, the weights are multiplied with IF data and summed over all elements to form 12 composite signals. These signals are then processed by composite tracking channels. Finally, positioning is performed if obtaining the pseudoranges and navigation messages from these channels. Figure 8 is the graphical user interface (GUI) of CRPA software receiver. It consists of channel statuses of all channels, carrier phase differences, positioning results, East-North (EN) plot, sky plot, Carrier to Noise (C/No) plot and gain patterns of array. The CRPA software receiver is tracking 10 satellites and its positioning history is shown in the EN plot. The beamforming channels have about 6 dB more gain on C/No than the channels of single element. In each pattern, the direction with highest gain corresponds to the direction of the satellite. While the CRPA software receiver is running, the carrier phase measurements of all elements and azimuth/elevation of satellites are logged every 100 msec. Each data set in table 2 is processed by software receiver to log the data.

CALCULATING ELECTRICAL LAYOUT OF ANTENNA ARRAY BY CARRIER PHASE PRECISE POSITIONING

The procedure of calculating the electrical layout of antenna array is depicted in figure 9. The single difference Integrated Carrier Phase (ICP) between signals of elements and reference element *j* is represented as [9]:

$$\varphi_{ij}^{k} = \lambda^{-1} r_{ij}^{k} + \delta L_{ij} + N_{ij}^{k} + \varepsilon_{ij}^{k} \tag{2}$$

where r_{ij} is differential range toward the k satellite between ith and jth antenna, N_{ij}^{k} is the integer associated to φ_{ij}^{k}, ε_{ij}^{k} is the phase error. The double difference ICP between satellites and reference satellite l is represented as:

$$\varphi_{ij}^{kl} = \lambda^{-1} r_{ij}^{kl} + N_{ij}^{kl} + \varepsilon_{ij}^{kl} \tag{3}$$

The cable length difference term is subtracted in the double difference. Based on the distance of the antenna position close to one wavelength, equation (3) can be written as:

$$\varphi_{ij}^{kl} = \lambda^{-1}\left(-\hat{r}^{k} - \left(-\hat{r}^{l}\right)\right) p_{ij} + N_{ij}^{kl} + \varepsilon_{ij}^{kl} \tag{4}$$

where $\hat{r}^{k}$ is the unit vector to satellite k, p_{ij} is baseline vector between ith and jth element. By combining all the double difference measurements of the pair ijth antennas, the observations equation is represented as:

$$\begin{bmatrix} \varphi_{ij}^{21} \\ \varphi_{ij}^{31} \\ \vdots \\ \varphi_{ij}^{K1} \end{bmatrix} = \lambda^{-1} \begin{bmatrix} -\hat{r}^{2} - \left(-\hat{r}^{1}\right) \\ -\hat{r}^{3} - \left(-\hat{r}^{1}\right) \\ \vdots \\ -\hat{r}^{K} - \left(-\hat{r}^{1}\right) \end{bmatrix} p_{ij} + I_{K-1} \cdot \begin{bmatrix} N_{ij}^{21} \\ N_{ij}^{31} \\ \vdots \\ N_{ij}^{K1} \end{bmatrix} + \begin{bmatrix} \varepsilon_{ij}^{21} \\ \varepsilon_{ij}^{31} \\ \vdots \\ \varepsilon_{ij}^{K1} \end{bmatrix} \tag{5}$$

$$\Gamma = \lambda^{-1} G p_{ij} + N + \mathrm{E}$$

From the positioning results of composite channels, the azimuth and elevation of satellites are used to manipulate matrix G. To solve equation (5), the LAMBDA method [10] is adopted to solve the integer vector N. Then, p_{ij} is solved by substituting N into equation (5). Finally, the cable length differences are obtained by substituting the solutions of N and p_{ij} into the equation (2).

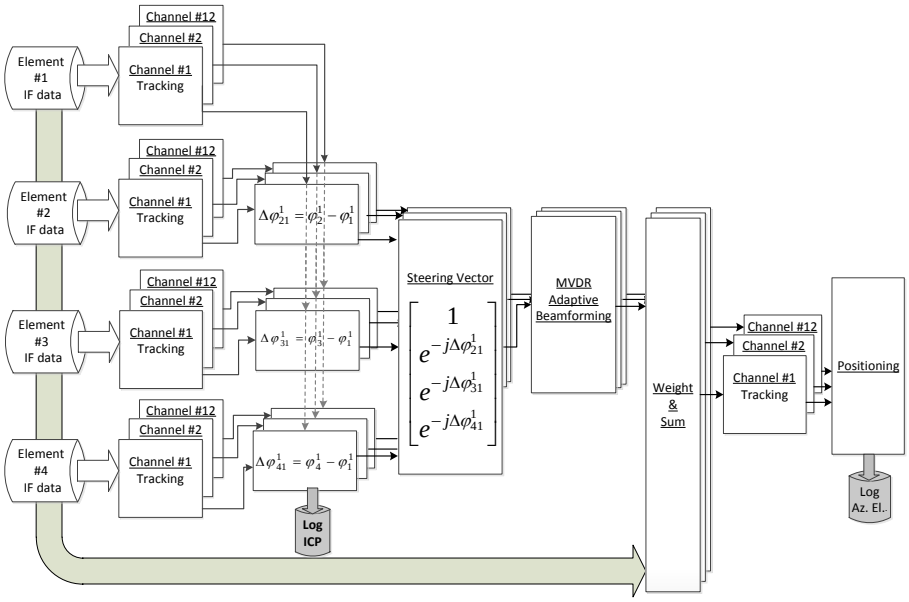

Figure 7. Block diagram of the software architecture

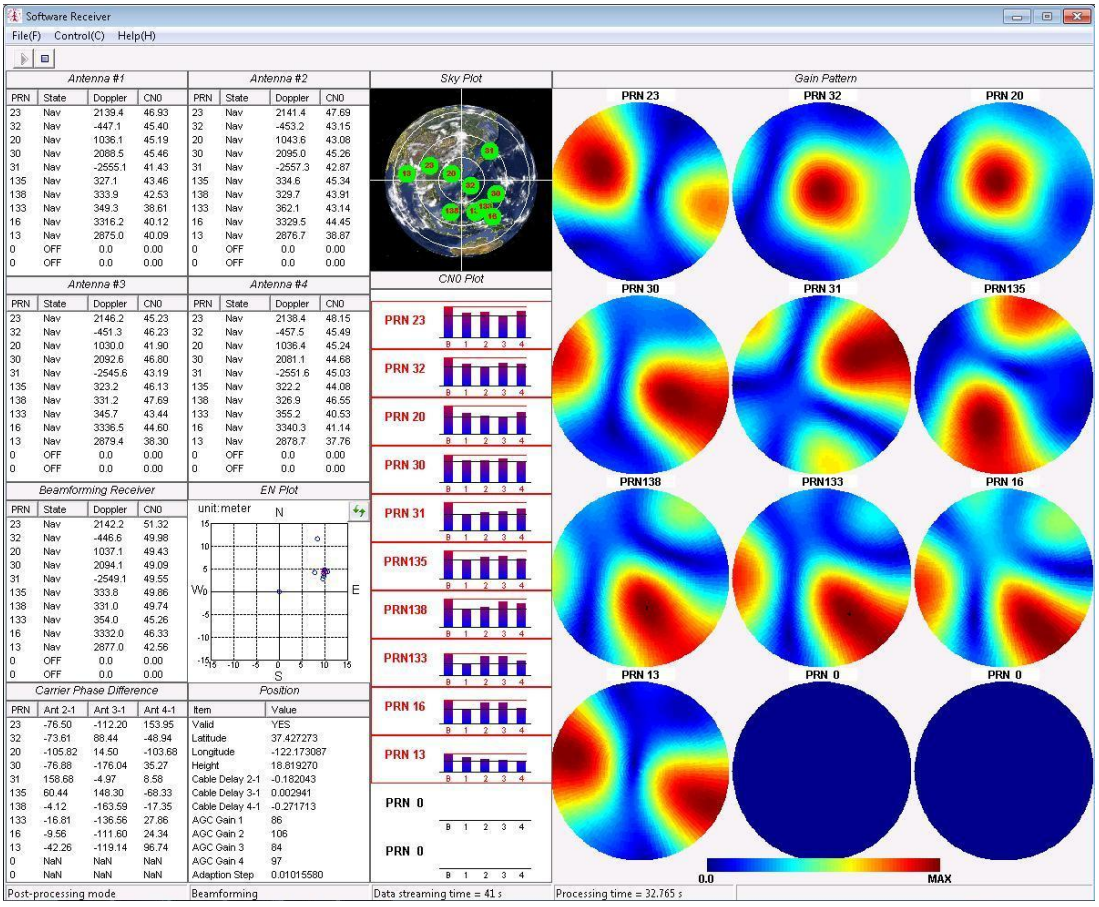

Figure 8. Screenshot of CRPA software receiver GUI

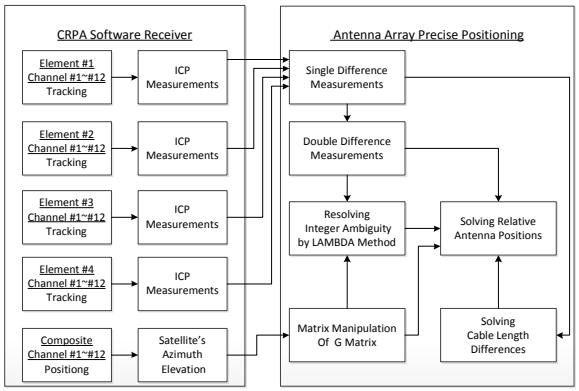

Figure 9. Procedure of calculating antenna array electrical spacing

This approach averages the pattern across all satellite measurements observed during the calibration period.

RESULTS OF ELECTRICAL LAYOUT OF ANTENNA ARRAYS

Using the procedure in the previous section, all electrical layouts of the antenna array are calculated and shown in figure 10 and 11. We align the vectors from element #1 to element #2 for all layouts. Table 3 lists the total difference between physical and electrical layouts. For the same model of antenna, the Y layout has less difference than square layout. And, in term of antenna model, the antenna #1 has the least difference for both Y and square layouts. We could conclude that the mutual coupling effect of Y layout is less than square layout, and the antenna #1 has less mutual coupling effect among all three models of antenna, for these particular elements and observations utilized.

Table 3. Total difference between physical and electrical layout

	Y layout	Square layout
Antenna #1	0.1286 λ	0.2001 λ
Antenna #2	0.2526 λ	0.3055 λ
Antenna #3	0.2175 λ	0.2347 λ

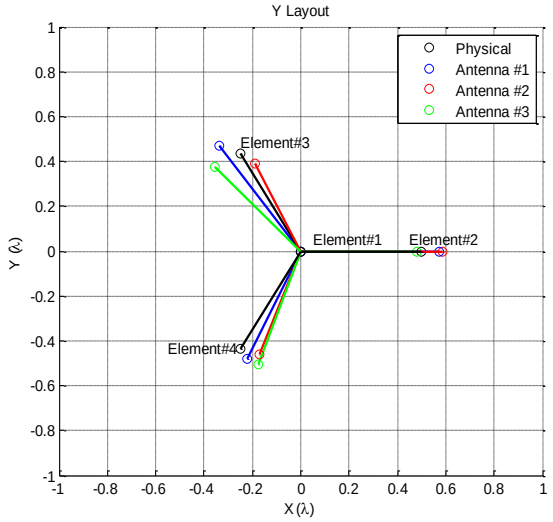

Figure 10. Results of electrical layout using three models of antenna compared to physical layout for Y layout

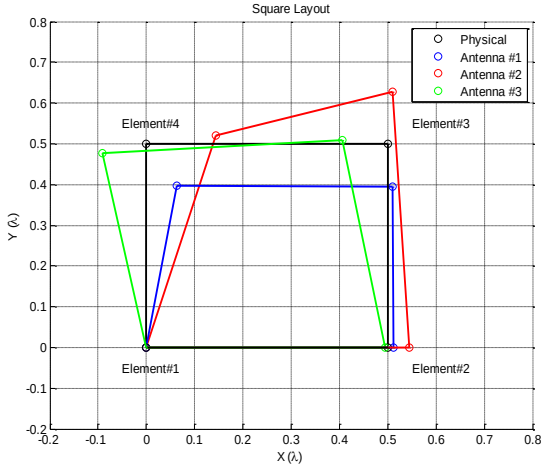

Figure 11. Results of electrical layout using three models of antenna compared to physical layout for square layout

In order to compare the patterns of all calculated electrical layouts, we select two directions 1) elevation 90 º 2) a target satellite WAAS GEO PRN138 which is available for all data sets. The results are shown in Figure 12 and 13, respectively. From the figure 12, the beamwidth of Y layout is narrower than square layout for all antenna models. When compared to figure 2, this result proves the analysis in the pattern analysis section. But, in the figure 13, a strong sidelobe appears azimuth -60º in the pattern of Y layout/antenna #2. If there is an interference located in this direction, the anti-interference perform will be limited. This is due to high mutual coupling effect of antenna #2 and only can be seen after calculating the electrical layout.

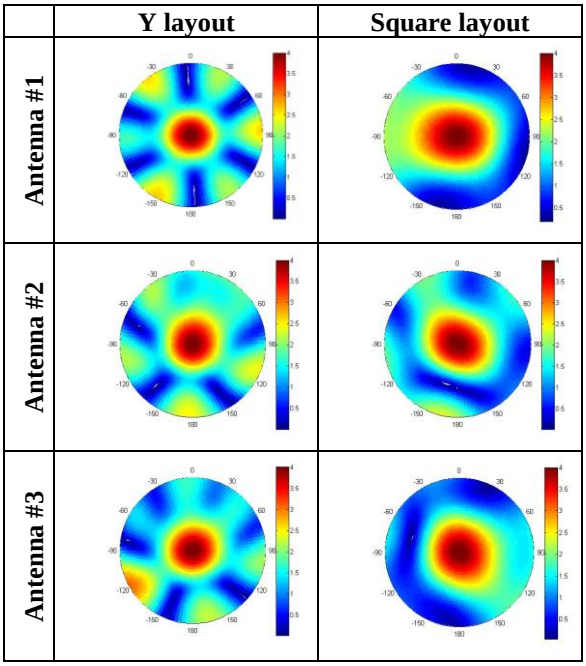

Figure 12. Patterns of three models of antenna and two layouts toward elevation 90 °

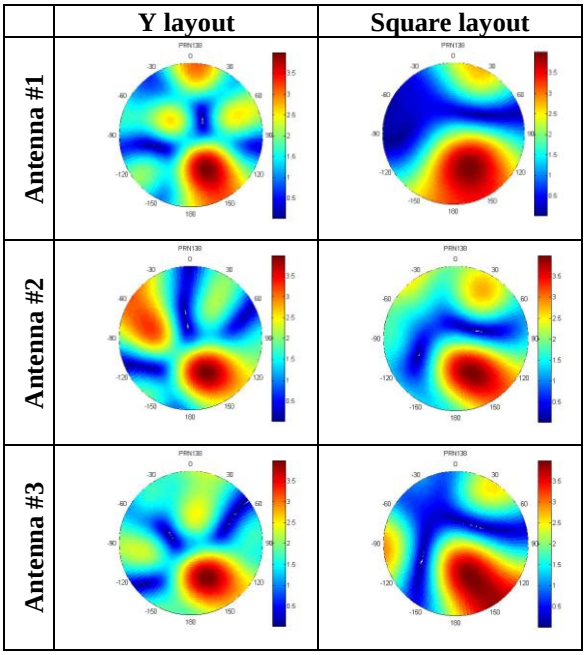

Figure 13. Patterns of three models of antenna and two layouts toward WAAS GEO PRN138

SUMMARY & CONCLUSIONS

A study of geometry is first conducted by analyzing the pattern of two selected half-wavelength layouts 1) Y and 2) square. The beamwidth of these layouts are compared and the result shows that the Y layout has narrower beamwidth. Narrow beamwidth will benefit the anti-interference performance if the interference source is close to the direction of target satellite. Then, three models of COTS antennas are selected to assemble the antenna array. The specifications of these antenna show all antennas have high gain LNA and great out-of-band rejection. However, no mutual coupling effect performances are not specified as these antennas are meant to function in a stand-alone manner. The signal collection hardware is built for collecting the array data sets at a data rate of 64 MB/s. This hardware then collected on air data for six different layout/antenna combinations. The data sets are then processed by our developed CRPA software receiver. This receiver logs the carrier phase measurements and azimuth/elevation information of satellites for over 100 seconds. These logging data is sent to differential carrier phase positioning to calculate the electrical layouts.

The results of electrical layout experiment show that the Y layout has less difference with respect to physical layout. That implies that the Y layout has less mutual coupling effect. For the antenna selection, the antenna model WS3978 showed the least difference between electrical and physical layout. And, its pattern does not have high grating lobe in the direction other than target satellite.

The hardware and methods used in this paper can be served as a testing tool for any antenna array. Specifically, the methodology developed here: 1) collect data 2) compare physical with electrical layout and 3) assess resultant antenna gain pattern allows us to compare performance and select the best antenna/layout combination. Results can be used to model mutual coupling and overall effect of layout/antenna on antenna gain pattern/CRPA capabilities. This procedure is especially important when using the COTS antennas to assemble antenna array and as we increase the number of antennas in and the geometry possibilities of the array

ACKNOWLEDGMENTS

The author gratefully acknowledges the works of Dr. Dennis M. Akos and Dr. Jiwon Seo for building the signal collection hardware. The author gratefully acknowledges the invaluable assistance of Dr. Jiwon Seo for collecting data sets. The author gratefully acknowledges the research guidance of Dr. Dennis M. Akos and Dr. Sherman Lo. The author gratefully acknowledges the invitation of Prof. Per Enge to visit GPS Lab at Stanford. The author also gratefully acknowledges the Federal Aviation Administration (FAA) CRDA 08-G-007 for supporting this research.

REFERENCES

[1] Y.-H. Chen, D. S. De Lorenzo, J. Seo, S. Lo, J.-C. Juang, P. Enge, and D. M. Akos, "Real-Time Software Receiver for GPS Controlled Reception Pattern Array Processing," Proceedings of ION GNSS 2010, 2010.

[2] M.V.T. Heckler, M. Cuntz, A. Konovaltsev, L.A. Greda, A. Dreher, M. Meurer, "Development of Robust Safety-of-Life Navigation Receivers," IEEE Transactions on Microwave Theory and Techniques, Volume 59, Issue 4, pp. 998-1005, 2011

[3] USRP2 motherboard and DBSRX2 programmable daughterboard, Ettus Research LLC, reachable on the web at http://www.ettus.com.

[4] R. C. Hansen, Phased Array Antennas, Second Edition, John Wiley & Sons, 2009

[5] WS3978, 3978D-HR and WS3997 datasheets, PCTEL Inc., reachable on the web at http://www.pctel.com/index.cgi

[6] U.S. Patent No. 7,305,021, "Real-Time Software Receiver," Awarded Dec. 4, 2007, by B.M. Ledvina, M.L. Psiaki, S.P. Powell, and P.M. Kintner, Jr.

[7] Y.-H. Chen and J.-C. Juang, "A GNSS Software Receiver Approach for the Processing of. Intermittent Data," Proceedings of ION GNSS 2007, 2007

[8] J. Seo, Y.-H. Chen, D. S. De Lorenzo, S. Lo, P. Enge, D. Akos, and J. Lee, "A Real-Time Capable Software-Defined Receiver Using GPU for Adaptive Anti-Jam GPS Sensors," Sensors, 2011

[9] P. Misra and P. Enge, Global Positioning System: Signals, Measurement, and Performance, 2nd Edition, Ganga-Jamuna Press, Lincoln, MA. , 2006

[10] P. de Jonge and C. Tiberius, "The LAMBDA Method for Integer Ambiguity Estimation: Implementation Aspects," Publications of the Delft Geodetic Computing Centre, 1996